Int. J. Multiphase Flow Vol. 17, No. 5, pp. 635–652, 1991
Printed in Great Britain.

0301-9322/91 $3.00 + 0.00

ANALYSIS OF PHASE DISTRIBUTION IN FULLY DEVELOPED LAMINAR BUBBLY TWO-PHASE FLOW

S. P. ANTAL,[1] R. T. LAHEY JR[2] and J. E. FLAHERTY[2]
[1]Knolls Atomic Power Laboratory, Schenectady, New York, U.S.A.
[2]Rensselaer Polytechnic Institute, Troy, NY 12180-3590, U.S.A.

(Received 11 July 1989; in revised form 1 May 1991)

Abstract—A two-fluid model of multidimensional laminar bubbly two-phase flow is developed and used to analyze vertical pipe flows. A Galerkin finite element method is utilized to perform the numerical evaluations. Good agreement is found with the available data when adequate models for the lateral lift force and wall force on the dispersed phase (i.e. the bubbles) are used.

Key Words: phase distribution, two-phase flow, two-fluid modelling

INTRODUCTION

A fundamental problem in multiphase flow is the prediction of the velocity and phase distribution for laminar bubbly two-phase flow in a pipe. Significantly, even for this well-defined problem no analytic solution has been developed which successfully predicts the data. Experiments performed by Nakoryakov *et al.* (1986), show a strong tendency for the bubbles to collect near a vertical pipe wall for cocurrent upflow. In contrast, for cocurrent downflow, no bubbles were found for a finite distance away from the wall and a relatively flat void profile was observed in the interior of the pipe. The purpose of this paper is to present a two-fluid model of laminar bubbly flow which predicts the observed void profiles for both cocurrent upflows and downflows.

This paper presents a new model for the force acting on a bubble near a wall. This wall-force prevents the bubbles from touching the wall. It is analogous to a lubrication force, i.e. the hydrodynamic force which floats a journal in its bearing housing. The main effect of the wall-force was to assure the zero void condition found experimentally near vertical walls, while not significantly effecting the phase distribution away from the wall.

In a previous study by Achard & Cartellier (1985) a two-fluid model was used to predict the void profile for laminar bubbly cocurrent upflow in a pipe. In their study the region near the wall was neglected and an analytical solution for the void fraction profile in the "core" region of a pipe was derived. Since all wall region phenomena were neglected the predicted void profile peaked at the wall rather than approached zero. Achard & Cartellier (1985) concluded that another kind of transverse force which repels bubbles away from the wall was needed.

Experimental work done by Valukina *et al.* (1979) has shown that the laminar bubbly flow void distribution problem can be quite complicated. For example, they found that by changing the bubble diameter, peaking of the void fraction near the wall may or may not occur.

The present study assumes that the flow is "laminar" (i.e. $Re_L < 1500$) and the local void fraction is low enough (e.g. $\epsilon < 10\%$) so that the cell model, to be discussed shortly, is valid. The analysis also assumes that the bubbles can be treated as spheres in the development of the various lateral forces.

TWO-FLUID MODELING

The analysis of multiphase flow can be done at various levels of complexity. These levels range from the use of homogeneous flow models to multidimensional two-fluid models. Among these models, the two-fluid formulation is considered to be the most accurate because of the explicit

treatment of the interaction between the phases. The two-fluid model is developed by first considering the conservation equations of each phase separately. Through the use of appropriate averaging techniques these conservation equations can be used to represent the macroscopic field of each phase. However, in the process of averaging, important characteristics of the flow field are lost and must be reintroduced into the model via appropriate closure laws. For this analysis, the two-fluid model proposed by Ishii (1975) was used. The general form of the two-fluid model for adiabatic air–water flow can be written as

$$\frac{\partial(\epsilon_k \rho_k)}{\partial t} + \nabla \cdot (\epsilon_k \rho_k \mathbf{v}_k) = 0 \qquad [1]$$

and

$$\frac{\partial(\epsilon_k \rho_k \mathbf{v}_k)}{\partial t} + \nabla \cdot (\epsilon_k \rho_k \mathbf{v}_k \mathbf{v}_k) = -\epsilon_k \nabla p_k + \nabla \cdot [\epsilon_k (\tau_k + \tau_k^{\mathrm{T}})] + (p_{ki} - p_k) \nabla \epsilon_k + \epsilon_k \rho_k \mathbf{g} + \mathbf{M}_{ki} - \tau_{ki} \cdot \nabla \epsilon_k. \qquad [2]$$

Here the subscript k denotes phase k (l = G for the gas phase; k = L for the liquid phase) and the subscript i stands for the value at the interface between the two phases. The time-averaged density, velocity, pressure, volume fraction, viscous shear and bubble-induced turbulence are given by ρ_k, $\mathbf{v}_k$, p_k, ϵ_k, τ_k and τ_k^{T}, respectively. The time-averaged interfacial momentum exchange, velocity, shear and pressure are denoted by $\mathbf{M}_{ki}$, $\mathbf{v}_{ki}$, τ_{ki} and p_{ki}, respectively.

For fully developed adiabatic air–water bubbly flow in a pipe the continuity equation reduces to the trivial solution of no net radial (r-direction) motion (i.e. $v_{\mathrm{G}} = v_{\mathrm{L}} = 0$). The time derivative and convective terms in the momentum equations are also zero for fully developed steady flow, thus the phasic momentum equation becomes:

$$-\epsilon_k \nabla p_k + \nabla \cdot [\epsilon_k (\tau_k + \tau_k^{\mathrm{T}})] + (p_{ki} - p_k) \nabla \epsilon_k + \epsilon_k \rho_k \mathbf{g} + \mathbf{M}_{ki} - \tau_{ki} \cdot \nabla \epsilon_k = 0. \qquad [3]$$

In the gas phase several additional simplifications can be used. For example, due to the relatively small viscosity and density of the gas phase compared with the liquid phase, the total shear and the $(p_{\mathrm{Gi}} - p_{\mathrm{G}})$ terms can be neglected.

Substituting these assumptions into [3] and noting that $\epsilon \equiv \epsilon_{\mathrm{G}} = (1 - \epsilon_{\mathrm{L}})$ yields:

$$0 = -\epsilon \nabla p_{\mathrm{G}} + \epsilon \rho_{\mathrm{G}} \mathbf{g} + \mathbf{M}_{\mathrm{Gi}} \qquad [4a]$$

and

$$0 = -(1 - \epsilon) \nabla p_{\mathrm{L}} + \nabla \cdot [(1 - \epsilon)(\tau_{\mathrm{L}} + \tau_{\mathrm{L}}^{\mathrm{T}})] + (p_{\mathrm{Li}} - p_{\mathrm{L}}) \nabla (1 - \epsilon) + (1 - \epsilon) \rho_{\mathrm{L}} \mathbf{g} + \mathbf{M}_{\mathrm{Li}} - \tau_{\mathrm{Li}} \cdot \nabla (1 - \epsilon). \qquad [4b]$$

At this point closure laws are required to relate terms such as $\mathbf{M}_{\mathrm{Gi}}$, $\mathbf{M}_{\mathrm{Li}}$, $\tau_{\mathrm{L}}^{\mathrm{T}}$, $(p_{\mathrm{Li}} - p_{\mathrm{L}})$ and τ_{Li} to the state variables $\mathbf{v}_{\mathrm{L}}$, $\mathbf{v}_{\mathrm{G}}$, p_{G}, p_{L} and ϵ. These constitutive equations (i.e. closure laws) must be accurately modeled for the two-fluid formulation to be useful. Except for the interfacial drag law, cell models (Nigmatulin 1979) were used in conjunction with potential flow theory to develop each closure law. Basically, the inviscid solution for flow around a sphere was used to approximate the flow around the bubbles in the flow field. A spherical cell was assumed to be centered around each bubble and extended into the liquid flow field so that the volumetric average of the gas phase to the total cell volume was equal to the local void fraction. By geometry the radius of the cell, R_{cell}, can be related to the void fraction and bubble radius, R_{b}, through (Nigmatulin 1979):

$$R_{\mathrm{cell}} = \frac{R_{\mathrm{b}}}{\epsilon^{1/3}}. \qquad [5]$$

A limited discussion of each closure law used in this analysis will be given below. For a more detailed treatment of any particular model the reader is referred to the references cited.

The interfacial momentum exchange, M_{ki}, can be partitioned into three terms: the axial interfacial drag, M_{ki}^{d}; the lateral lift-force, M_{ki}^{L}; and the wall-force, M_{ki}^{W}. The interfacial drag law was taken from Ishii & Mishima (1984):

$$\mathbf{M}_{Gi}^{d} = -\mathbf{M}_{Li}^{d} = -\frac{3}{8}\frac{\epsilon}{R_b} C_D \rho_L (\mathbf{v}_G - \mathbf{v}_L)|\mathbf{v}_G - \mathbf{v}_L|, \quad [6]$$

where

$$C_D = \frac{24}{\mathrm{Re}_{2\phi}}(1 + 0.1\,\mathrm{Re}_{2\phi}^{0.75}),$$

$$\mathrm{Re}_{2\phi} = \frac{2R_b \rho_L (\mathbf{v}_G - \mathbf{v}_L)}{\mu_m}$$

and

$$\mu_m = \frac{\mu_L}{(1-\epsilon)}.$$

The lift-force on a bubble has been previously calculated by Drew & Lahey (1987) and Zun (1980). This force is perpendicular to the rotation vector and the bubble's velocity vector. The general form for the lift-force can be written as

$$\mathbf{M}_G^L = -\mathbf{M}_L^L = C_L \epsilon \rho_L (\mathbf{v}_L - \mathbf{v}_G) \times (\nabla \times \mathbf{v}_L). \quad [7]$$

Here C_L is the lift coefficient and can range from about 0.01 to 0.5 (Wang *et al.* 1987).

When a rising bubble comes in close proximity to a wall the normally uniform drainage of the fluid around the bubble changes dramatically. The no-slip condition at the wall slows the drainage rate between the bubble and the wall which in turn increases the drainage rate on the opposite side. The net effecxt of this asymmetry is to create a hydrodynamic force which acts to drive the bubble away from the wall. Unfortunately, no analytical three-dimensional solution of the flow between a bubble and a wall is available to describe this phenomena. However, an approximate two-dimensional solution can be derived for flow between a cylinder and a wall. This solution was used to deduce the functional form of the wall-force on a sphere. Appendix A presents the details of the derivation of this wall-force and shows that it is of the form:

$$\mathbf{M}_G^W = -\mathbf{M}_L^W = \frac{\epsilon \rho_L |u_\parallel|^2}{R_b}\left[C_{W1} + C_{W2}\left(\frac{R_b}{y_0}\right)\right]\mathbf{n}_W, \quad [8]$$

where

$$\mathbf{u}_\parallel = (\mathbf{v}_G - \mathbf{v}_L) - [\mathbf{n}_W \cdot (\mathbf{v}_G - \mathbf{v}_L)]\mathbf{n}_W$$

$$C_{W1} = -0.104 - 0.06 U_R$$

and

$$C_{W2} = 0.147.$$

Here y_0 is the distance between the bubble and the wall and $\mathbf{n}_W$ is the unit outward normal vector on the surface of the wall.

The next closure laws which require modeling are the viscous and bubble-induced shear stresses, τ_L and τ_L^T, respectively. A Newtonian shear law was assumed for the viscous shear stress in the liquid phase. The bubble-induced turbulence accounts for the perturbations of the liquid flow around each bubble due to fluid displacement. To obtain this perturbation the potential flow solution for flow around a sphere was divided into the macroscopic mean motion and the induced pseudo-turbulent fluctuations. A detailed cell model derivation of this term has been given previously by Nigmatulin (1979):

$$\tau_L^T = -\epsilon \rho_L \left[\tfrac{3}{20}|\mathbf{v}_G - \mathbf{v}_L|^2 \mathbf{I} + \tfrac{1}{20}(\mathbf{v}_G - \mathbf{v}_L)(\mathbf{v}_G - \mathbf{v}_L)\right]. \quad [9]$$

The next closure law required for this analysis is a model for the term which relates the area-averaged interfacial pressure to the spatial average pressure of the liquid phase, $(p_{Li} - p_L)$. This term represents a Bernoulli effect in the liquid flow field. Near the side surfaces of each bubble the local fluid speed is higher than the far field speed due to the deflection of the flow around the bubble. The Bernoulli equation implies that this increase in speed is accompanied by a decrease in the local pressure. Thus, the average pressure on the surface of the bubble is less than the far field pressure. Stuhmiller (1977) used the potential flow solution for flow around a sphere to deduce that this pressure difference is

$$p_{Li} - p_L = -\tfrac{1}{4}\rho_L(1-\epsilon)|\mathbf{v}_G - \mathbf{v}_L|^2. \tag{10a}$$

In contrast, to a good first approximation,

$$p_{Gi} - p_G = 0. \tag{10b}$$

Another closure law required for this analysis is to relate the local gas phase pressure to the local liquid phase pressure. This can be done through a momentum jump condition across the interface. The pressure difference can then be grouped into three parts: the pressure difference, $p_{Gi} - p_G$, in the gas phase; the pressure difference, $p_{Gi} - p_{Li}$, across the gas–liquid interface; and the pressure drop in the liquid phase, $p_{Li} - p_L$. As noted in [10b] the pressure difference in the gas phase is small and can be neglected. By assuming spherical bubbles the pressure change across the interface is accounted by the surface tension, σ. Equation [10a] can be used to account for the pressure change in the liquid phase. Combining these terms results in the overall gas to liquid phase pressure difference:

$$(p_G - p_L)\mathbf{I} = \frac{2\sigma}{R_b}\mathbf{I} + (p_{Li} - p_L)\mathbf{I} - \boldsymbol{\tau}_{Li}. \tag{11a}$$

Two assumptions for the interfacial shear stress tensor, τ_{Ki}, are commonly used. Either this term is set equal to zero, or it is assumed to be equal to the total shear stress in the liquid at the surface of the bubble (i.e. $\boldsymbol{\tau}_{Li} = \boldsymbol{\tau}_L + \boldsymbol{\tau}_L^T$, evaluated at the surface of the bubble). Let us assume that the interfacial shear stress tensor, τ_{Li}, can be constituted using a Newtonian shear law and [9] evaluated at the interface:

$$\boldsymbol{\tau}_{Li} = \mu_L \nabla \mathbf{v}_L - \rho_L\left[\frac{3}{20}|\mathbf{v}_G - \mathbf{v}_L|^2\mathbf{I} + \frac{1}{20}(\mathbf{v}_G - \mathbf{v}_L)\cdot(\mathbf{v}_G - \mathbf{v}_L)\mathbf{I}\right]. \tag{11b}$$

Substituting [9] and [11b] into [11a] yields the momentum jump condition:

$$(p_G - p_L)\mathbf{I} = \frac{2\sigma}{R_b}\mathbf{I} - \tfrac{1}{4}\rho_L|\mathbf{v}_G - \mathbf{v}_L|^2(1-\epsilon)\mathbf{I} - \mu_L\nabla\mathbf{v}_L + \tfrac{3}{20}\rho_L|\mathbf{v}_G - \mathbf{v}_L|^2\mathbf{I} + \tfrac{1}{20}(\mathbf{v}_G - \mathbf{v}_L)\cdot(\mathbf{v}_G - \mathbf{v}_L)\mathbf{I}. \tag{11c}$$

With all the closure laws specified, the complete description of the two-fluid model of steady laminar bubbly flow can now be written as:

gas phase momentum,

$$-\epsilon\nabla p_G + \epsilon\rho_G\mathbf{g} - \frac{3}{8}\frac{\epsilon}{R_b}C_D\rho_L(\mathbf{v}_G - \mathbf{v}_L)|\mathbf{v}_G - \mathbf{v}_L| - C_L\epsilon\rho_L(\mathbf{v}_G - \mathbf{v}_L)\times(\nabla\times\mathbf{v}_L) + \frac{\epsilon\rho_L|\mathbf{U}_\parallel|^2}{R_b}\left[C_{W1} + C_{W2}\left(\frac{R_b}{y_0}\right)\right]\mathbf{n}_W = 0; \tag{12a}$$

liquid phase momentum,

$$-(1-\epsilon)\nabla p_L + \nabla\cdot\{(1-\epsilon)[\mu_L\nabla\mathbf{v}_L - \epsilon\rho_L(\tfrac{3}{20}|\mathbf{v}_G - \mathbf{v}_L|^2\mathbf{I} + \tfrac{1}{20}(\mathbf{v}_G - \mathbf{v}_L)(\mathbf{v}_G - \mathbf{v}_L))]\}$$
$$-\tfrac{1}{4}\rho_L|\mathbf{v}_G - \mathbf{v}_L|^2(1-\epsilon)\nabla\epsilon + (1-\epsilon)\rho_L\mathbf{g} + C_L\epsilon\rho_L(\mathbf{v}_L - \mathbf{v}_G)\times(\nabla\times\mathbf{v}_L)$$
$$-\frac{\epsilon\rho_L|\mathbf{u}_\parallel|^2}{R_b}\left[C_{W1} + C_{W2}\left(\frac{R_b}{y_0}\right)\right]\mathbf{n}_W + \frac{3}{8}\frac{\epsilon}{R_b}C_D\rho_L(\mathbf{v}_G - \mathbf{v}_L)|\mathbf{v}_G - \mathbf{v}_L|$$
$$-[\mu_L\nabla\mathbf{v}_L - \rho_L[\tfrac{3}{20}|\mathbf{v}_G - \mathbf{v}_L|^2\mathbf{I} + \tfrac{1}{20}(\mathbf{v}_G - \mathbf{v}_L)\cdot(\mathbf{v}_G - \mathbf{v}_L)]]\cdot\nabla\epsilon = 0; \tag{12b}$$

and

interface jump condition,

$$(p_G - p_L)\mathbf{I} = \frac{2\sigma}{R_b}\mathbf{I} - \tfrac{1}{4}\rho_L|\mathbf{v}_G - \mathbf{v}_L|^2(1-\epsilon)\mathbf{I} - \mu_L\nabla\mathbf{v}_L + \tfrac{3}{20}\rho_L|\mathbf{v}_G - \mathbf{v}_L|^2\mathbf{I} + \tfrac{1}{20}(\mathbf{v}_G - \mathbf{v}_L)\cdot(\mathbf{v}_G - \mathbf{v}_L)\mathbf{I}. \quad [12c]$$

Note that the last term in [12b] represents a force due to interfacial shear stress. As stated earlier, this term was modeled in two ways; either it was set equal to the total shear stress (as written) or was set equal to zero.

The boundary conditions for steady fully developed laminar bubbly flow are as follows:

- No-slip condition at the wall for the continuous phase (i.e. we assume it is the liquid which wets the wall).
- The channel-average void fraction, $\langle\epsilon\rangle$.
- The axial pressure gradient, $\partial p_L/\partial z = \partial p_G/\partial z$.

Note that a no-slip condition at the wall for the vapor phase cannot be prescribed since vapor viscosity has been neglected.

It is also worth noting that the local void fraction at the pipe wall was not included in the set of boundary conditions even though experimental data shows that zero void fraction occurs at the wall for bubbly flows. In the next section it will be shown that prescribing the wall void fraction results in an overconstrained set of equations. Indeed, zero wall void fraction, which has been observed experimentally, is a natural result of the force on the bubbles rather than being applied as a boundary condition.

NUMERICAL SIMULATION

Since an exact solution of the set of nonlinear partial differential equations given by [12a–c] is not possible, a numerical method was required. The Galerkin finite element method was chosen since it provides a robust procedure for solving differential equations of the boundary value type. The procedure employs subdivision of the solution domain into many smaller regions and uses approximation theory to quantize the behavior of the equations over each finite element. To better understand the finite element simulation the conservation equations have been rewritten explicitly for the axisymmetric cylindrical geometry shown in figure 1:

$$\epsilon\frac{\partial p_G}{\partial z} = \epsilon\rho_G g - \frac{3}{8}\frac{\epsilon}{R_b}C_D\rho_L U_R|U_R|, \quad [13a]$$

$$\epsilon\frac{\partial p_G}{\partial r} = -C_L\epsilon\rho_L U_R\frac{\partial u_L}{\partial r} - \frac{\epsilon\rho_L U_R^2}{R_b}\left[C_{W1} + C_{W2}\left(\frac{R_b}{y_0}\right)\right], \quad [13b]$$

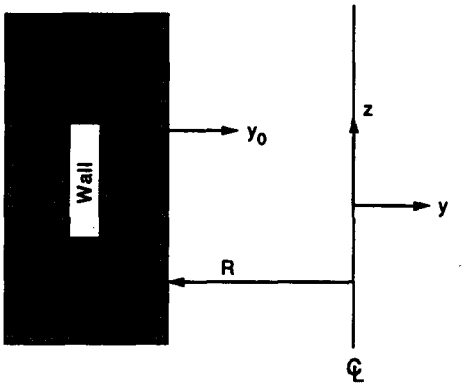

Figure 1. Axisymmetric pipe for numerical simulation.

$$(1-\epsilon)\frac{\partial p_L}{\partial z}=\frac{1}{r}\frac{\partial}{\partial r}\left[r(1-\epsilon)\mu_L\frac{\partial u_L}{\partial r}\right]+\frac{3}{8}\frac{\epsilon}{R_b}C_D U_R|U_R|+(1-\epsilon)\rho_L g_z+\mu_L\frac{\partial u_L}{\partial r}\frac{\partial \epsilon}{\partial r}, \quad [13c]$$

$$(1-\epsilon)\frac{\partial p_L}{\partial r}=-\frac{\partial}{\partial r}\left[\tfrac{3}{20}\rho_L\epsilon(1-\epsilon)U_R^2\right]+C_L\epsilon\rho_L U_R\frac{\partial u_L}{\partial r}+\tfrac{1}{4}\rho_L(1-\epsilon)U_R^2\frac{\partial \epsilon}{\partial r}$$
$$+\frac{\epsilon\rho_L U_R^2}{R_b}\left[C_{W1}+C_{W2}\left(\frac{R_b}{y_0}\right)\right]-\tfrac{3}{20}\rho_L U_R^2\frac{\partial \epsilon}{\partial r} \quad [13d]$$

and

$$p_G-p_L=\frac{2\sigma}{R_b}-\tfrac{1}{4}(1-\epsilon)\rho_L U_R^2\frac{\partial \epsilon}{\partial r}. \quad [13e]$$

Here U_R is the relative velocity in the axial direction and u_L is the axial velocity of the liquid phase. By combining [13b], [13c] and [13e] the radial gas and liquid pressure gradient can be eliminated, resulting in an expression which describes the radial void profile. This does not effect the accuracy of the solution and the lateral pressure field can be recovered as a post-processing step. The simplified set of equations which can be used to solve for the velocity and void profile are:

$$\epsilon\frac{\partial p_G}{\partial z}=\epsilon\rho_G g-\frac{3}{8}\frac{\epsilon}{R_b}C_D\rho_L U_R|U_R|, \quad [14a]$$

$$(1-\epsilon)\frac{\partial p_L}{\partial z}=\frac{1}{r}\frac{\partial}{\partial r}\left[r(1-\epsilon)\mu_L\frac{\partial u_L}{\partial r}\right]+\frac{3}{8}\frac{\epsilon}{R_b}C_L U_R|U_R|+(1-\epsilon)\rho_L g+\mu_L\frac{\partial u_L}{\partial r}\frac{\partial \epsilon}{\partial r} \quad [14b]$$

and

$$\epsilon\frac{\partial}{\partial r}\left[\tfrac{3}{20}\epsilon(1-\epsilon)\rho_L U_R^2\right]-C_L\rho_L\epsilon U_R\frac{\partial u_L}{\partial r}-\tfrac{1}{2}\epsilon(1-\epsilon)U_R^2\frac{\partial \epsilon}{\partial r}$$
$$-\frac{\epsilon\rho_L U_R^2}{R_b}\left[C_{W1}+C_{W2}\left(\frac{R_b}{y_0}\right)\right]+\tfrac{3}{20}\epsilon\rho_L U_R^2\frac{\partial \epsilon}{\partial r}=0. \quad [14c]$$

At this point it should be noted that the void fraction in [14a] can be cancelled from each term leaving an algebraic expression for the relative velocity, U_R. Since the axial pressure gradient is constant for fully developed flows, the relative velocity will be constant for uniform bubble size. Therefore, for a given axial pressure gradient, $\partial p_G/\partial z$, [14a] was used to evaluate the relative velocity.

The remaining equations, [14b] and [14c], require three boundary conditions as specified below.

The axial liquid momentum equation [14b] is a second-order elliptic partial differential equation and therefore requires two boundary conditions. One of the boundary conditions to be applied is the no-slip condition at the wall. The combined vapor and liquid transverse momentum equation, [14c] is a first-order differential equation and can satisfy one boundary condition. For this analysis the average void fraction in the pipe, $\langle\epsilon\rangle$, was chosen for the boundary condition.

If the wall void fraction is also specified then [14c] is over constrained and in general does *not* have a solution. The wall void fraction can be obtained by taking the limit of [14c] as y_0 (i.e. the local distance from the wall) approaches zero. It should be noted that since y_0 is the distance from the bubble's center to the wall it is limited by the bubble radius. However, since the bubble radius is very small compared to the pipe diameter the limit of y_0 approaching zero is useful in physically explaining the behavior of the void profile near the wall. If we assume that the void fraction and velocity profiles are well behaved (i.e. not multivalued functions) then the only term which can be very large is the wall-force. Applying the limit to this term yields:

$$\lim_{y_0\to 0}\left(C_{W2}\frac{\epsilon\rho_L U_R^2}{R_b}\frac{R_b}{y_0}\right)=\lim_{y_0\to 0}\left(C_{W2}\frac{\epsilon\rho_L U_R^2}{y_0}\right)=0. \quad [14d]$$

Since, as discussed previously, the relative velocity is a constant then the local void fraction must approach zero at a rate $>y_0$ in order to satisfy [14c] and [14d]. The solution of zero void fraction automatically satisfies [14c] since the void fraction appears in each term. Physically, zero void fraction is the single-phase case where no transverse forces are present. Therefore, we find that zero

wall void fraction is a natural result of the lateral forces rather than an imposed boundary condition.

FINITE ELEMENT ANALYSIS

In order to numerically evaluate [14b] and [14c], they were discretized by a finite element method and used to update the radial liquid and void fraction profiles.

The theory behind the Galerkin finite element method is available in many texts (e.g. Wait & Mitchell 1985) and will not be repeated here. Only a brief outline of the method for this particular application will be presented below.

Linear basis functions were used to approximate the liquid velocity and void fraction profiles. The pipe was divided into N elements over which the variables were defined by

$$u_L = \sum_{n=1}^{N} u_{L_n} \theta_n \qquad [15a]$$

and

$$\epsilon = \sum_{n=1}^{N} \epsilon_n \theta_n. \qquad [15b]$$

Here θ_n is a linear hat function with coefficients given by u_{L_n} and ϵ_n. Employing the procedure for the Galerkin finite element method [14a–d] were multiplied by a weight function, W, and integrated over the domain of interest. Next, each integral was divided into a sum of integrals over each finite element, this results in the following set of equations:

$$\sum_{n=1}^{N} \left[\int_{A_n} (1-\epsilon) \frac{\partial p_L}{\partial z} W \, dA \right] = \sum_{n=1}^{N} \left\{ \int_{A_n} \frac{1}{r} \frac{\partial}{\partial r} \left[r(1-\epsilon) \mu_L \frac{\partial u_L}{\partial r} \right] W \, dA \right.$$
$$\left. + \int_{A_n} \frac{3}{8} \frac{\epsilon}{R_b} C_D U_R |U_R| W \, dA + \int_{A_n} (1-\epsilon) \rho_L g W \, dA + \int_{A_n} \mu_L \frac{\partial u_L}{\partial r} \frac{\partial \epsilon}{\partial r} W \, dA \right\} \qquad [16a]$$

and

$$\sum_{n=1}^{N} \left\{ \int_{A_n} \epsilon \frac{\partial}{\partial r} [\tfrac{1}{5} \epsilon (1-\epsilon) \rho_L U_R^2] W \, dA - \int_{A_n} C_L \rho_L \epsilon U_R \frac{\partial u_L}{\partial r} W \, dA - \int_{A_n} \tfrac{1}{2} \epsilon (1-\epsilon) U_R \frac{\partial \epsilon}{\partial r} W \, dA \right.$$
$$\left. - \int_{A_n} \frac{\epsilon \rho_L U_R^2}{R_b} \left[C_{W1} + C_{W2} \left(\frac{R_b}{y_0} \right) \right] W \, dA + \int_{A_n} \tfrac{3}{20} \epsilon \rho_L U_R^2 \frac{\partial \epsilon}{\partial r} W \, dA \right\} = 0. \qquad [16b]$$

The definitions of the variables u_L and ϵ, given by [15a, b] were introduced into [16a, b]. The integration was then performed element-by-element with the results summed together so as to satisfy [16a, b]. In order to obtain a linear set of algebraic equations a standard Newton–Raphson linearization technique was used on any nonlinear term.

Next, the boundary conditions were imposed on the set of discretized algebraic equations. The particular boundary conditions appropriate for this analysis are

$$u_{L_1} = 0$$

and

$$\sum_{n=1}^{N+1} \Delta_n \epsilon_n = R \langle \epsilon \rangle,$$

where u_{L_1} is the liquid phase velocity at the wall and $\langle \epsilon \rangle$ specifies the global void fraction in the pipe; the element spacing is given by Δ_n and the pipe radius by R.

The final step in the numerical simulation was to solve the discretized algebraic equations along with their boundary conditions. Since the number of equations involved in this simulation is relatively small, a direct matrix inversion technique was used. The basic form of the resulting matrices was tridiagonal for the cases considered here. Therefore, a classic forward elimination and backward substitution technique was used to invert the matrix.

Table 1. Experimental data for laminar bubbly flow (Nakoryakov *et al.* 1986, 1987)

Fluids	Pressure	Pipe dia (cm)	Liquid phase Re	Bubble dia (mm)	Area average void fraction $\langle \epsilon \rangle$
Air–water	Atmospheric	1.5	1267.0	0.87	1.9%

In practice, [16a] and [16b] were alternatively solved using guessed values for the liquid phase velocity and void fraction and then updated. After the first few attempts at this method it became obvious that a very strong coupling existed between the velocity and void fraction fields. Without any two-dimensional or temporal terms (particularly the virtual mass force) oscillations quickly developed and the solution diverged. In order to control this coupling without adding artificial terms underrelaxation was used in the void profile calculation.

RESULTS

Accurate experimental data for laminar bubbly air–water flow is very limited. One available set of data has been reported by Nakoryakov *et al.* (1986, 1987). Unfortunately, most of the data was taken at higher liquid phase Re values (i.e. >2000). One data set was taken at a liquid Re = 1276

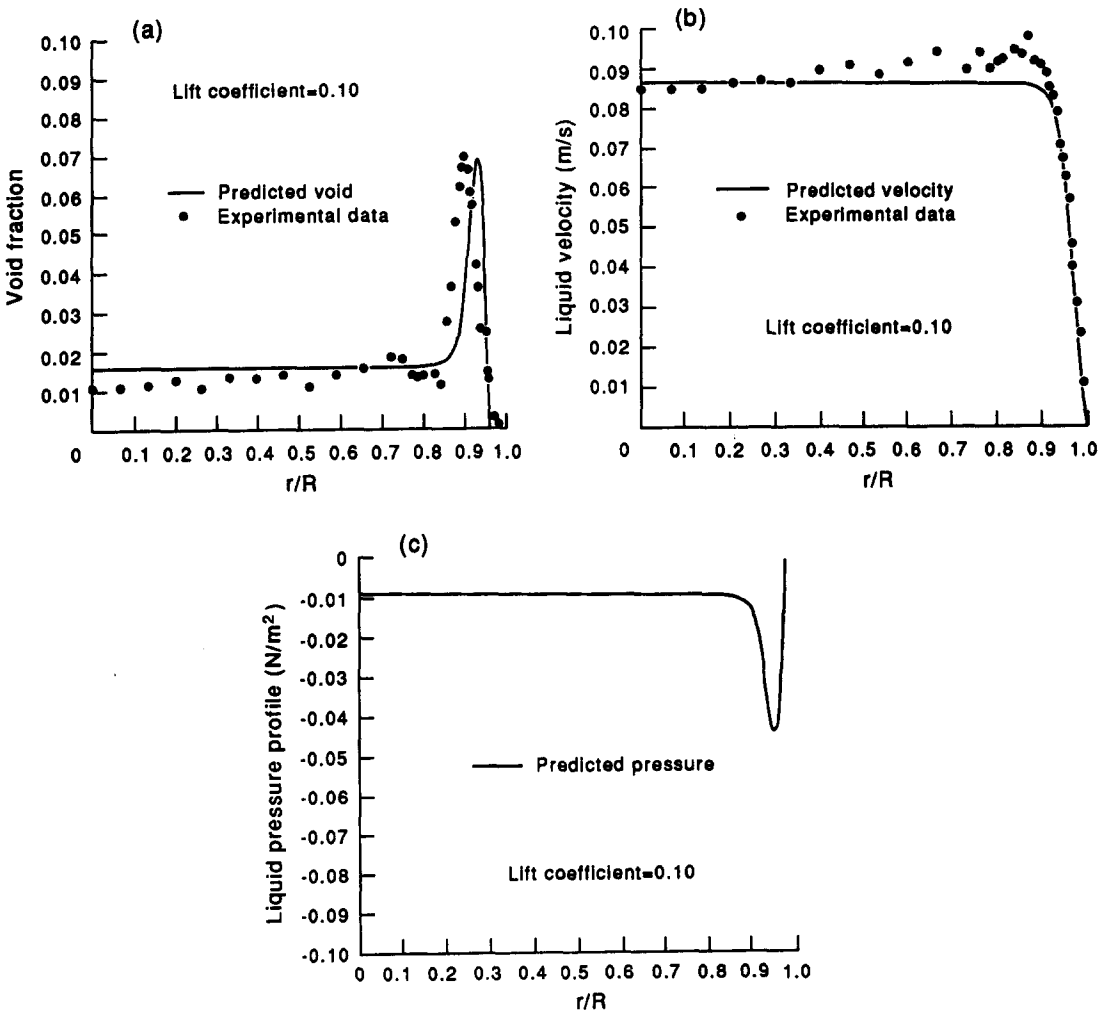

Figure. 2. (a) Void fraction profile for cocurrent upflow; $Re_L = 1276$, $p_0 = 1$ atm, $U_R = 0.1$ m/s. (b) Liquid velocity profile for cocurrent upflow; $Re_L = 1276$, $p_0 = 1$ atm, $U_R = 0.1$ m/s. (c) Liquid pressure profile $(p_0 - p_L)$ for cocurrent upflow; $Re_L = 1276$, $p_0 = 1$ atm, $U_R = 0.1$ m/s.

and was used to test two-fluid model predictions. The important geometrical and controlling parameters for this lower Re data set are given in table 1.

The lateral lift coefficient ranges from 0.01 to 0.5 (Wang *et al.* 1987). For the conditions of this experiment a value of 0.1 appeared to be appropriate and was used.

Figures 2a–c show the numerical results for the cocurrent upflow case listed in table 1. Note that for this case the interfacial shear stress, τ_{Li}, was set equal to the total shear stresss at the surface of the bubble in the liquid phase. As shown in figure 2a, the void fraction profile is strongly skewed toward the wall. The experimental data taken by Nakoryakov *et al.* (1986) are also shown in figure 2a. The predicted profile agrees quite well with the trends found experimentally. However, one discrepancy worth noting is that the location of zero void fraction is predicted at an r/R of about 0.96, while the experimental measurements show the void fraction goes to zero closer to the wall. This is just a consequence of using a discrete approximation of the continuous two-fluid model's partial differential equations. The cell model was developed for a bubble near a wall, however, the resulting net force is assumed to occur at the center of the bubble. Therefore, errors up to the size of the cell model are inherent in the model.

Figure 2b compares the liquid phase velocity profile predicted by the two-fluid model against measured data. The void peaking near the wall creates a high shear rate in the liquid phase near the wall. In fact, the liquid velocity profile is rather similar to a turbulent single-phase velocity profile. That is, a small boundary layer exists near the wall followed by relatively uniform velocity in the interior of the flow field. Figure 2c shows the predicted liquid pressure field. The pressure field was determined during post processing of the velocity and void results. Appendix B details a derivation of the pressure calculation. The lateral pressure profile presented in figure 2c shows a local pressure reduction near the wall where the peak void fraction occurs. This pressure "well" near the wall is similar to what happens in turbulent two-phase flows in which the shear-induced turbulence creates a local pressure decrease where the velocity fluctuations of the continuous phase

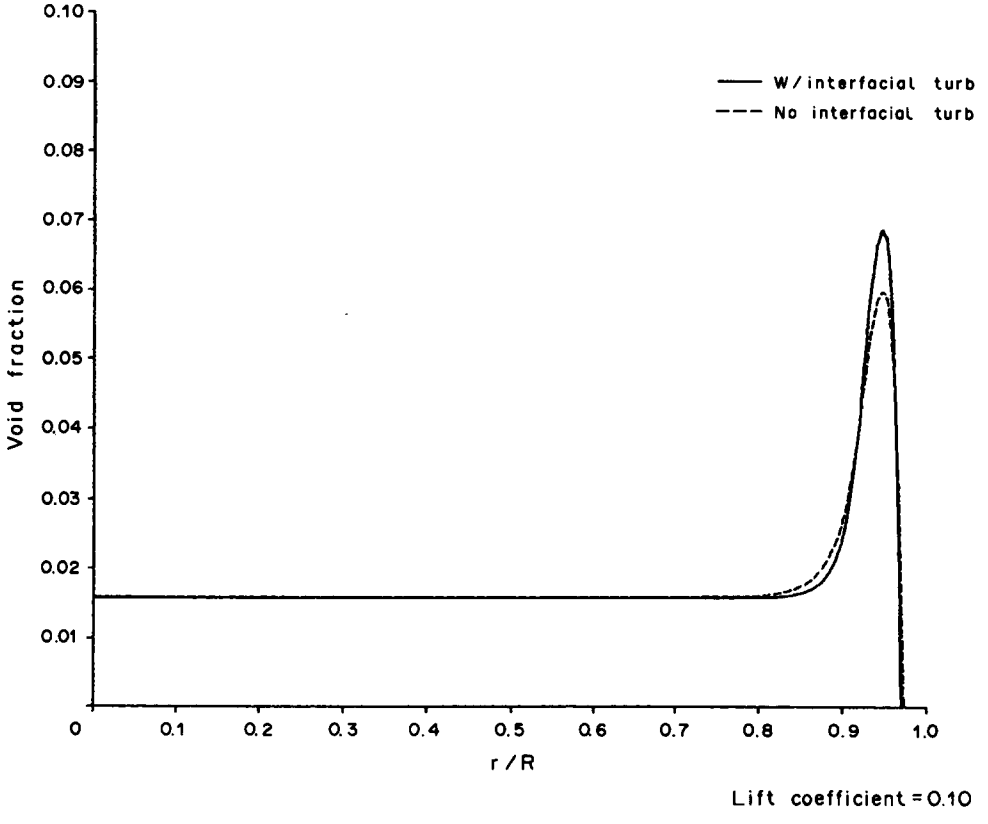

Figure 3a. Void fraction profile with the without the interfacial shear model; $Re_L = 1276$, $p_0 = 1$ atm, $U_R = 0.1$ m/s.

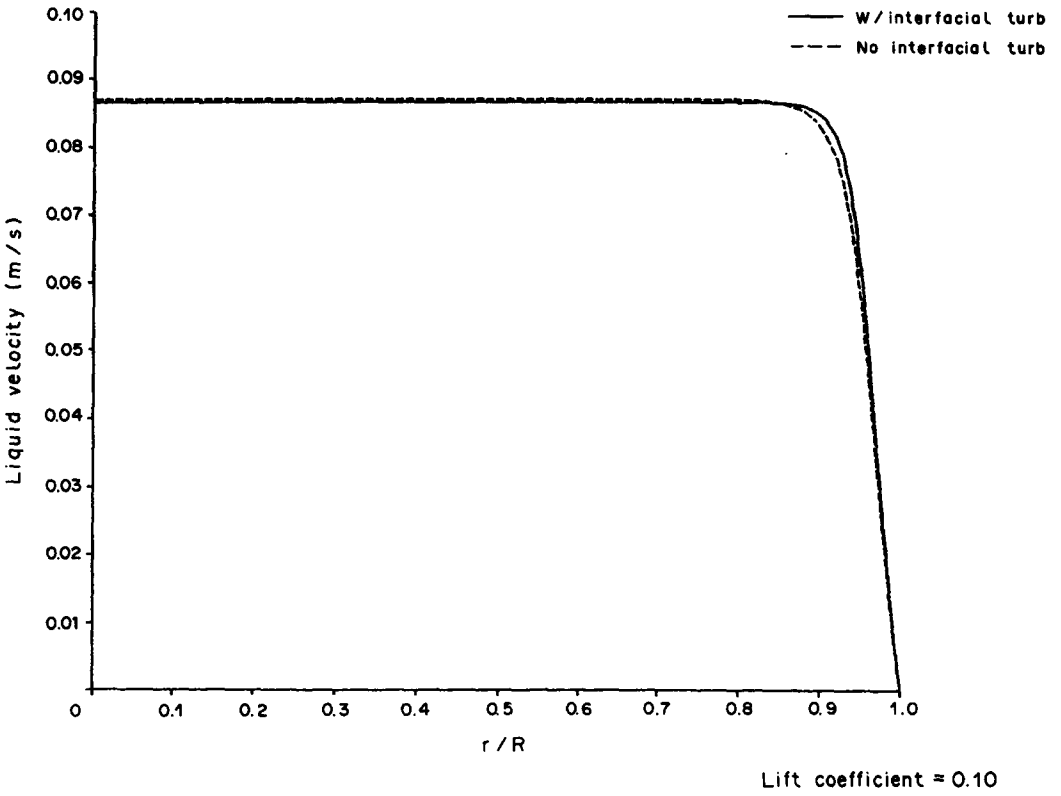

Figure 3b. Liquid velocity profile with and without the interfacial shear model; $Re_L = 1276$, $p_0 = 1$ atm, $U_R = 0.1$ m/s.

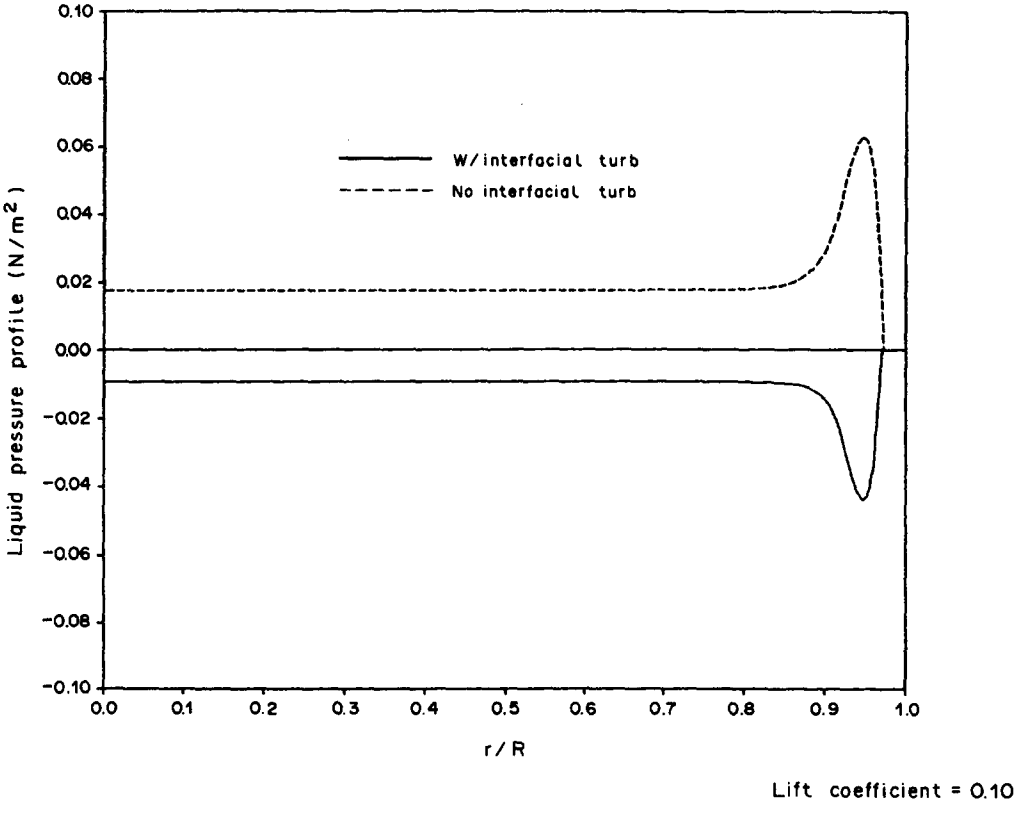

Figure 3c. Liquid pressure profile ($p_0 - p_L$) with and without the interfacial shear model; $Re_L = 1276$, $p_0 = 1$ atm, $U_R = 0.1$ m/s.

are the largest (Wang *et al.* 1987). It should be noted that the location of the peak void fraction occurs where the lift-force is balanced by the wall-force. Moreover, the magnitude of the void fraction at the peak location is controlled by the bubble-induced turbulence level and the local Bernoulli effect (i.e. the $(p_{Li} - p_L)$ term of [4b]). The Bernoulli effect causes a decrease in liquid pressure near the sides of the bubble due to the increased liquid velocity there. Therefore, at higher void fractions the Bernoulli pressure difference is small and a higher cell-averaged pressure is predicted. However, the combination of both the bubble-induced turbulence terms, τ_L^T and τ_{Li}^T of [4b], dominate the Bernoulli eflect and a net pressure reduction results for the case shown.

The same test case was rerun with the interfacial shear term, τ_{Li}, set equal to zero. A comparison of the results with and without the interfacial shear term is shown in figures 3a–c. In figure 3a, the void fraction profiles are compared. It can be noted that the effect of the interfacial term is to increase the peak void level but not change its location. This effect can also be seen in [14c]. The last term on the l.h.s. represents the contribution from the interfacial shear. Since it only contains the spatial derivative of the void fraction it can only modify its gradient. The location of the peak can be determined from a balance of the lift and wall-forces. Balancing these terms gives

$$C_L \rho_L U_R^2 \epsilon \frac{\partial u_L}{\partial r} = \frac{\rho_L U_R^2 \epsilon}{R_b}\left[C_{W1} + C_{W2}\left(\frac{R_b}{y_0}\right)\right].$$

However, this equation cannot be solved directly since the liquid velocity must be given by [14b].

The velocity profiles, figure 3b, are nearly identical for both modeling assumptions. The major difference can be seen in the local pressure profiles given in figure 3c. Without the interfacial shear term the bubble-induced turbulence term, τ_L^T, cannnot dominate the Bernoulli effect. Therefore, as shown in figure 3c, a local pressure increase is predicted where the void fraction profile peaks. This result is in agreement with simulations of turbulent phase distribution phenomena (Lopez de Bertodano *et al.* 1990).

A sensitivity study to the value of the lift-force coefficient used is presented in figure 4. The coefficient of [7] was varied from 0.05 to 0.15. As expected, the larger the value of the coefficient

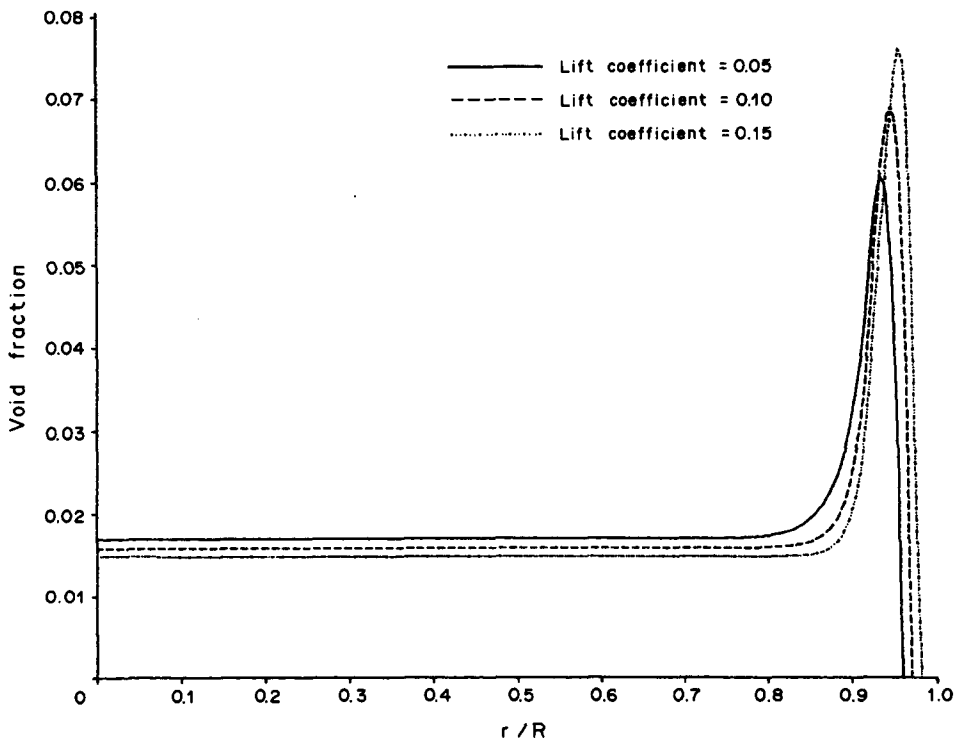

Figure 4. Sensitivity of the void fraction profile to the value of the lift-force coefficient.

the closer to the wall the peak void fraction occurred. This new peak void fraction location represents a re-balancing of the larger lift-force with an equally larger wall-force. It is interesting to note that since the bubbles are "closer" to the wall for the larger lift-force coefficient and the same number of bubbles are present then the peak value of void fraction must increase. This peak value of void fraction varied from 6.0% for the 0.05 lift-force coefficient to approx. 7.5% for the 0.15 lift-force coefficient.

Another numerical simulation was performed using the conditions in table 1 for a vertical downflow run. The same lift and wall-force coefficient were used as for the run shown in figure 3. The results of the downflow simulation are shown in figures 5a–c. The predictions show void coring in the interior of the pipe and a zero void fraction near the wall. For cocurrent downflow, both the lift and wall-force are directed toward the center of the pipe and therefore no wall-peaking in the void profile is observed. These same trends have been observed in turbulent bubbly flow experiments by Wang *et al.* (1987) and Nakoryakov *et al.* (1987). Unfortunately, laminar bubbly downflow data was not available, but similar trends are expected.

SUMMARY AND CONCLUSIONS

A two-fluid model of laminar bubbly two-phase flow was developed in order to predict the phase distribution in a circular pipe. The use of a two-fluid model allows a detailed description of the lateral forces acting on the bubbles to be developed. For fully developed laminar bubbly flow two

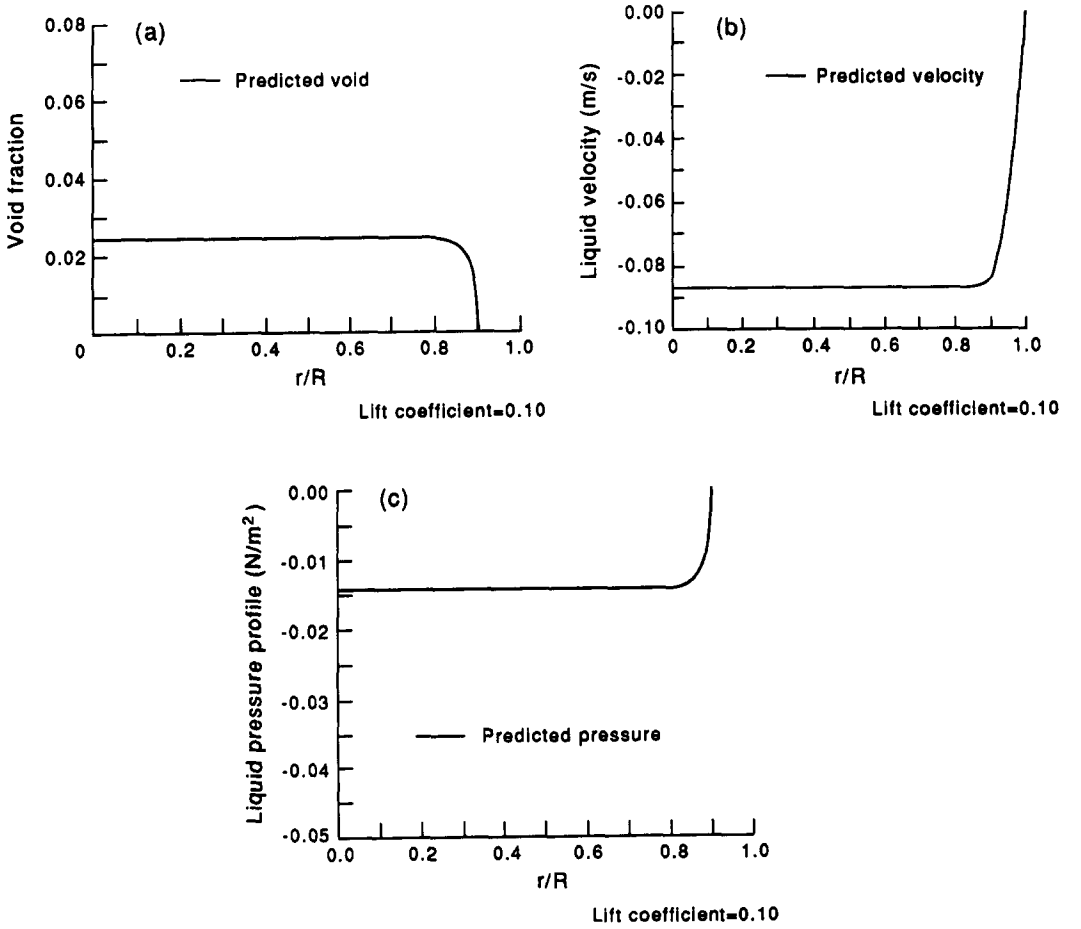

Figure 5. (a) Void fraction profile for countercurrent downflow; $Re_L = 1276$, $p_0 = 1$ atm, $U_R = 0.1$ m/s. (b) Liquid velocity profile for countercurrent downflow; $Re_L = 1276$, $p_0 = 1$ atm, $U_R = 0.1$ m/s. (c) Liquid velocity profile for countercurrent downflow; $Re_L = 1276$, $p_0 = 1$ atm, $U_R = 0.1$ m/s.

forces are shown to control the void fraction profile, they are: a lateral lift-force and a wall-force (appendix A). The lift-force is similar in nature to the aerodynamic lift of an airfoil, but differs in that it is the result of a gradient in the velocity field over a symmetric bubble rather than a uniform flow over an asymmetric airfoil. The wall-force acts to keep the bubbles away from the pipe wall. This wall-force is analogous to wall forces in lubrication theory.

Numerical simulation of the two-fluid model using a finite element technique showed that the balance between the lift and wall-force determines the void fraction profile. For upflows of positive buoyant bubbles the lift-force is directed toward the wall while the wall-force keeps the bubbles away from the wall. The result is a local peaking of the void fraction near the wall. For downflow of positive buoyant bubbles both the lift- and wall-force are directed toward the center of the pipe. As a result, no peaking of the void fraction is predicted. The peaking of the void fraction near the wall has been observed in experimental measurements of both laminar and turbulent two-phase bubbly upflows. The flat void profile in the interior of the pipe has been observed in turbulent two-phase bubbly downflows and is expected to occur in laminar flows as well.

The level of the peak void fraction was found to be controlled by the bubble-induced turbulence and the Bernoulli, $(p_{Li} - p_L)\nabla\epsilon$, terms. The bubble-induced turbulence tends to resist the increase in void level while the Bernoulli effect reinforces the buildup. However, the net effect of these terms is to resist the increase in void level.

Unlike single-phase laminar flow the radial pressure profile is not uniform. Depending on the model used for the interfacial turbulence term, τ_{Li}, the local pressure was found to either increase or decrease as the local void fraction increased. Unfortunately, experimental data was not available to clarify the actual trend in the pressure profile. Clearly more experimental work is needed to properly assess the models used in this analysis.

REFERENCES

ACHARD, J. L. & CARTELLIER, A. 1985 Local characteristics of upward bubbly flows. *PhysicoChem. Hydrodynam.* **6,** 841–852.

DREW, D. A. & LAHEY, R. T. JR 1987 The virtual mass and lift force on a sphere in rotating and straining inviscid flow. *Int. J. Multiphase Flow* **13,** 113–121.

ISHII, M. 1975 *Thermo-fluid Dynamic Theory of Two-phase Flow.* Eyrolles, Paris.

ISHII, M. & MISHIMA, K. 1984 Two-fluid modeling and hydrodynamic constitutive relations. *Nucl. Engng Des.* **82,** 107.

LOPEZ DE BERTODANO, M., LEE, S-J., LAHEY, R. T. JR & DREW, D. A. 1990 The predictions of two-phase turbulence and phase distribution phenomena using a Reynolds stress model. *J. Fluids Engng* **112,** 107–113.

NAKORYAKOV, V. E. *et al.* 1986 Study of upward bubbly flow at low liquid velocities. *Izv. sib. Otdel. Akad. Nauk SSSR.* **16,** 15–20.

NAKORYAKOV, V. E. *et al.* 1987 Study of downward bubbly flow in a vertical pipe. *Zh. prikl. Mekh. tekh. Phys.* **1,** 69–73.

NIGMATULIN, R. I. 1979 Spatial averaging in the mechanics of heterogeneous and dispersed systems. *Int. J. Multiphase Flow* **4,** 353–385.

SPALDING, D. B. 1986 *PHOENICS—Beginner's Guide and User Manual.* CHAM TR/100.

STUHMILLER, J. H. 1977 The influence of interfacial pressure on the character of two-phase flow model equations. In *ASME Symp. on Computational Techniques for Non-equilibrium Two-phase Phenomena,* p. 118.

VALUKINA, N. V., KOV'MENKO, B. K. & KASHINSKII, O. K. 1979 Characteristics of a flow of monodispersed gas–liquid mixture in a vertical tube. *Inzh. fiz. Zh.* **36**(4), 695.

WAIT, R. & MITCHELL, A. R. 1985 *Finite Element Analysis and Applications.* Wiley-Interscience, New York.

WANG, S. K., LEE, S. J., JONES, O. C. JR & LAHEY, R. T. JR 1987 3-D turbulence structure and phase distribution measurements in bubbly two-phase flows. *Int. J. Multiphase Flow* **13,** 327–343.

ZUN, I. 1980 The transverse migration of bubbles influenced by walls in vertical bubbly flow. *Int. J. Multiphase Flow* **6,** 583–588.

APPENDIX A

Derivation of the Wall-force

While an exact analytic expression has not yet been found for the hydrodynamic force on a moving bubble near a fixed wall, an estimate can be obtained in the following manner.

Consider the flow past two cylinders moving at velocity U, whose radii are R_0 and whose centers are separated by a distance $2y_0$. If a circulation of equal but opposite strength, Γ, is placed on these cylinders, the streamlines have the pattern shown in figure A1. By virtue of symmetry, the line of $y = 0$ can be taken as a fixed boundary so that the half of the plane represents the flow past a cylinder moving along a fixed wall. The flow field is approximated by the complex potential function

$$\omega = U\left[Z + R_0^2\left(\frac{1}{Z - iy_0} + \frac{1}{Z + iy_0}\right) + i\frac{\Gamma}{U}\ln\left(\frac{Z - iy_0}{Z + iy_0}\right)\right]. \qquad [A.1]$$

The circulation gives rise to a force which acts away from the wall transverse to the main flow stream. The calculation of this force is greatly facilitated through the use of Blasius's theorem, which is given by

$$X + i\Psi = \frac{i\rho_L}{2}\oint\left(\frac{d\omega}{d\bar{Z}}\right)^2 dZ. \qquad [A.2]$$

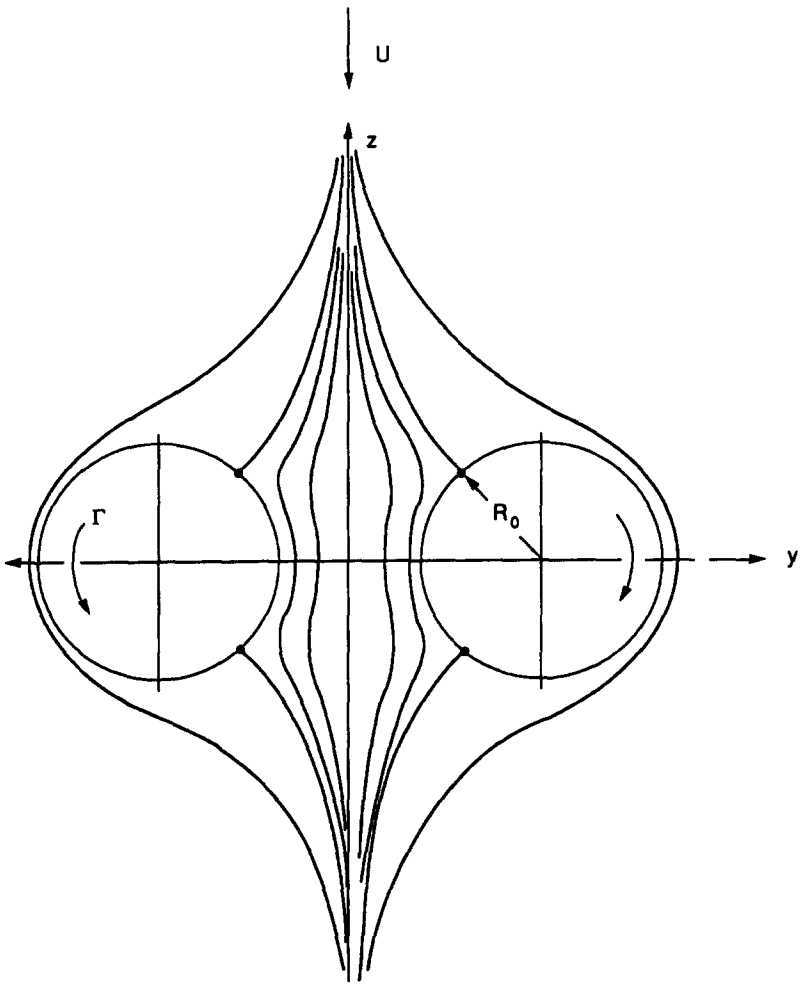

Figure A1. Streamlines of flow past two cylinders with an applied circulation.

Substitution of [A.1] into [A.2] and application of Cauchy's residue theorem leads to the result:

$$\Psi = 2\pi\rho_L U^2\left[\frac{\Gamma}{U}\left(1+\frac{R_0^2}{2y_0^2}\right)-\frac{R_0^4}{4y_0^3}-\frac{\Gamma^2}{2y_0U^2}\right]. \qquad [A.3]$$

Inspection of [A.3] shows that if the circulation is set equal to zero the resultant force is directed toward the wall and is due to the increased velocity between the wall and the cylinder. The force component due to the addition of circulation can therefore be considered as the potential flow equivalent of the force arising from the viscous slow down of the fluid between the wall and the cylinder due to the no-slip condition on the wall.

The strength of the circulation is determined so that the liquid velocity on the surface of the bubble satisfies the no-slip condition where the bubble touches the wall and approaches the free stream value when the bubble is far from the wall. That is, when the cylinder is far from the wall the circulation applied is zero and when the cylinder touches the wall the liquid velocity at the point of contact satisfies the no-slip condition. The axial liquid velocity (u_L) along the $z = 0$ axis of figure A1 is given by

$$u_L = -U\left[1+\frac{R_0^2}{(y-y_0)^2}+\frac{R_0^2}{(y+y_0)^2}+\frac{\Gamma}{U(y-y_0)}-\frac{\Gamma}{U(y+y_0)}\right]. \qquad [A.4]$$

Here u_L is the liquid velocity in the axial (z) direction and y is the distance from the wall.

Let us make the choice,

$$\Gamma = \frac{R_0^{n+1}(3U-u_G)}{2y_0^n}, \qquad [A.5]$$

where n is a constant to be evaluated later. Combining [A.5] with [A.4] yields

$$u_L = -U\left[1+\frac{R_0^2}{(y-y_0)^2}+\frac{R_0^2}{(y+y_0)}+\frac{R_0^{n+1}(3U-u_G)}{U2y_0^n(y-y_0)}-\frac{R_0^{n+1}(3U-u_G)}{2Uy_0^n(y+y_0)}\right]. \qquad [A.6]$$

Far from the wall ($y\to\infty$; $y_0 = y + R_0$) the liquid velocity approaches the free stream value:

$$\lim_{y\to\infty} u_L = -2U.$$

When the cylinder touches the wall ($y = 0$; $y_0 = R_0$) the liquid velocity at the point of contact becomes

$$u_L = -u_G.$$

This is the no-slip condition in our frame of reference. That is, for our Lagrangian point of view the bubble is stationary and the wall is traveling at a velocity of $-u_G$.

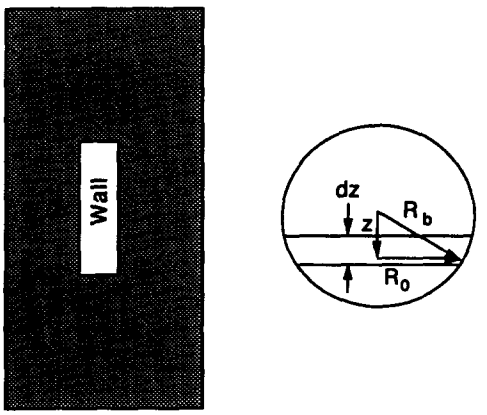

Figure A2. Integration of the "thin slice" wall-force over a three-dimensional bubble.

The force given by [A.3] can be assumed to apply to a "thin slice" of a three-dimensional bubble. To obtain the total force [A.3] is integrated over the surface of the spherical bubble to approximate the net force. Assuming that [A.3] applies over each "slice" of the sphere shown in figure A2 (i.e. neglecting end effects) the integrated wall force, F_W, can be evaluated from

$$F_W = \int_{-R_b}^{R_b} \Psi(z)\,dz. \qquad [A.7]$$

The integration of [A.7] can be greatly facilitated by noting that on the surface of the sphere the following relation is valid:

$$R_0^2 + z^2 = R_b^2. \qquad [A.8]$$

Using [A.8] to change the independent variable from z to R_0 in [A.7] gives:

$$F_W = 2\int_0^{R_b} \Psi(R_0)\frac{R_0\,dR_0}{\sqrt{R_b^2 - R_0^2}}. \qquad [A.9]$$

Substituting [A.3] and [A.5] into [A.7] and performing the integration yields:

$$F_W = 4\pi\rho_L U^2\left[\frac{\lambda_{n+2}R_b^{n+2}(3U-u_G)}{2y_0^n U} + \frac{\lambda_{n+4}R_b^{n+4}(3U-u_G)}{4y_0^{n+2}U} - \frac{\lambda_5 R_b^5}{4y_0^3} - \frac{\lambda_{2n+3}R_b^{2n+3}(3U-u_G)^2}{8y_0^{2n+1}U^2}\right]. \qquad [A.10]$$

Here λ_n is a constant given by

$$\lambda_n = \begin{cases} \dfrac{\pi}{2}\displaystyle\prod_{i=0}^{(n-2)/2}\left(\frac{n-2i-1}{n-2i}\right), & \text{if } n \text{ is even} \\ \displaystyle\prod_{i=0}^{(n-3)/2}\left(\frac{n-2i-1}{n-2i}\right), & \text{if } n \text{ is odd.} \end{cases}$$

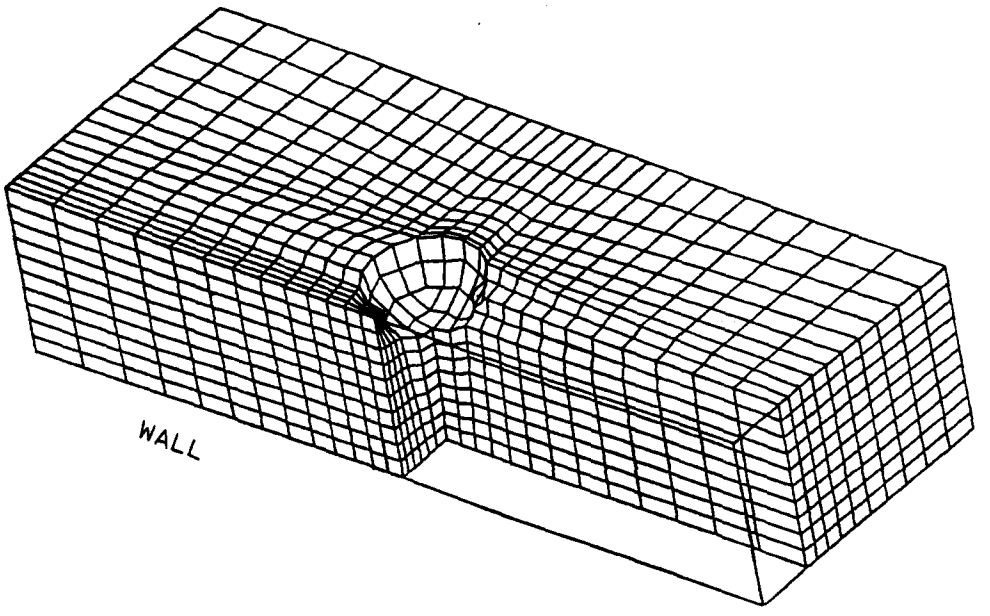

Figure A3. Grid used for flow past a bubble near a wall.

Near the wall, where the wall-force is important, the liquid velocity is small compared with the relative velocity due to the no-slip condition at the wall. Using the above observation and substituting the relations: $U = -U_R$, $3U - u_G = -4U_R - u_L \cong -4U_R$ into [A.10] yields:

$$F_W = 4\pi\rho_L U_R^2\left(\frac{2\lambda_{n+2}R_b^{n+2}}{y_0^n} + \frac{\lambda_{n+4}R_b^{n+4}}{y_0^{n+2}} - \frac{\lambda_5 R_b^5}{4y_0^3} - \frac{2\lambda_{2n+3}R_b^{2n+3}}{y_0^{2n+1}}\right). \quad [A.11]$$

The closure law required for a two-fluid model is a volumetric force and, therefore, [A.11] must be divided by the effective volume occupied by the bubble. For consistency with other models used in this analysis a cell model was assumed. The effective volume occupied by the bubble was determined from the definition of the local void fraction:

$$\epsilon = \frac{V_G}{V_{eff}},$$

where

$$V_G = \tfrac{4}{3}\pi R_b^3.$$

Dividing [A.11] by V_{eff}, the volumetric wall-force, $M^{(W)}$, is evaluated as

$$M^{(W)} = \frac{\epsilon\rho_L U_R^2}{R_b}\left[6\lambda_{n+2}\left(\frac{R_b}{y_0}\right)^n + 3\lambda_{n+4}\left(\frac{R_b}{y_0}\right)^{n+2} - \frac{3\lambda_5}{4}\left(\frac{R_b}{y_0}\right)^3 - 6\lambda_{2n+3}\left(\frac{R_b}{y_0}\right)^{2n+1}\right]. \quad [A.12]$$

The wall-force given in [A.12] was derived using several simplifying assumptions (e.g. inviscid flow theory) and therefore it cannot be directly used to calculate the repelling force, but only to give the appropriate form of the wall-force closure law. In order to evaluate the exponent, n, in [A.12], a Taylor series expansion of the term in the brackets was performed. The resulting constants were evaluated by comparison to a three-dimensional direct numerical simulation of viscous flow past a single bubble. Expanding the bracketed term in [A.12] about $y_0 = R_b$ gives:

$$\left[6\lambda_{n+2}\left(\frac{R_b}{y_0}\right)^n + 3\lambda_{n+4}\left(\frac{R_b}{y_0}\right)^{n+2} - \frac{3\lambda_5}{4}\left(\frac{R_b}{y_0}\right)^3 - 6\lambda_{2n+3}\left(\frac{R_b}{y_0}\right)^{2n+1}\right] = C_{W1} + C_{W2}\left(\frac{R_b}{y_0}\right) + C_{W3}\left(\frac{R_b}{y_0}\right)^2 + \cdots. \quad [A.13]$$

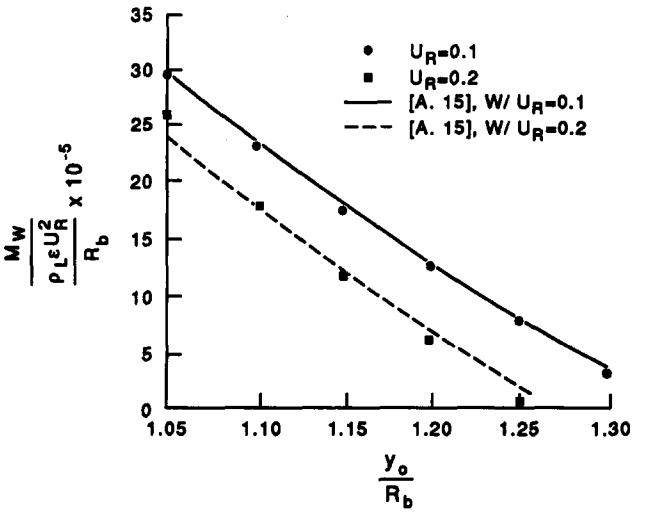

Figure A4. Normalized wall force, [A.15], compared with single bubble results (PHOENICS).

Combining [A.12] and [A.13] yields:

$$M^{(W)} = \frac{\epsilon \rho_L U_R^2}{R_b}\left[C_{W1} + C_{W2}\left(\frac{R_b}{y_0}\right) + C_{W3}\left(\frac{R_b}{y_0}\right)^2 + \cdots\right]. \quad [A.14]$$

In order to evaluate the constants in [A.14] the PHOENICS computer code (Spalding 1986) was used to model three-dimensional viscous flow around a bubble near a wall. A schematic of the grid used is shown in figure A3. The resulting pressure field was integrated over the surface of the bubble giving the wall-force. A uniform inlet flow was used so that lift-forces due to gradients in the liquid velocity field would be avoided. The resulting wall-force for two relative velocities ($U_R = 0.1$ and 0.2 m/s) is shown in figure A4.

The first two terms in [A.14] were found to satisfactorily fit the numerical results. The wall-force closure law used in the analysis of laminar bubbly flow is given by

$$M^{(W)} = \frac{\epsilon \rho_L U_R^2}{R_b}\left[C_{W1} + C_{W2}\left(\frac{R_b}{y_0}\right)\right], \quad [A.15]$$

where

$$C_{W1} = -0.06 U_R - 0.104$$

and

$$C_{W2} = 0.147.$$

This model of the wall-force is compared against the numerical results in figure A4. Good agreement can be noted.

APPENDIX B

Derivation of the Radial Pressure Distribution

The radial lift-force and wall-force can be eliminated by adding together [4a] and [4b], resulting in

$$\epsilon \nabla p_G + (1-\epsilon)\nabla p_L = \nabla \cdot [(1-\epsilon)\tau_L + \tau_L^T)] + (p_{Li} - p_L)\nabla(1-\epsilon) - \tau_{Li} \cdot \nabla(1-\epsilon) + \epsilon \rho_G \mathbf{g} + (1-\epsilon)\rho_L \mathbf{g}. \quad [B.1]$$

The radial component of [B.1] is

$$\frac{\partial p_L}{\partial r} + \epsilon\left(\frac{\partial p_G}{\partial r} - \frac{\partial p_L}{\partial r}\right) = \frac{\partial}{\partial r}[(1-\epsilon)\tau_{L_{rr}}^T] - (p_{Li} - p_L)\frac{\partial \epsilon}{\partial r} + \tau_{Li_{rr}}\frac{\partial \epsilon}{\partial r}. \quad [B.2]$$

The interfacial momentum jump condition for spherical bubbles can be written as

$$p_G - p_L = \frac{2\sigma}{R_b} + (p_{Li} - p_L) - \tau_{Li_{rr}}^T. \quad [B.3]$$

Here R_b is the radius of the bubble and σ is the surface tension. Differentiating [B.3] and combining with [B.2] yields:

$$\frac{\partial p_L}{\partial r} = \frac{\partial}{\partial r}[(1-\epsilon)\tau_{L_{rr}}^T] - \frac{\partial[\epsilon(p_{Li} - p_L)]}{\partial r} + \frac{\partial(\epsilon \tau_{Li_{rr}}^T)}{\partial r}. \quad [B.4]$$

Integrating [B.4] yields:

$$p_L - p_{Ref} = (1-\epsilon)\tau_{L_{rr}}^T - \epsilon(p_{Li} - p_L) + \epsilon \tau_{Li_{rr}}^T. \quad [B.5]$$

Here p_{Ref} is a constant of integration which was arbitrarily set equal to zero. Using [9] and [10] and setting τ_{Li}^T equal to the bubble-induced turbulence level on the surface of the sphere results in the following expression for local liquid phase pressure:

$$p_L = -\tfrac{1}{20}\epsilon \rho_L (u_G - u_L)^2 - \tfrac{1}{10}\epsilon^2 \rho_L (u_G - u_L)^2. \quad [B.6]$$

In contrast, if the interfacial turbulence term is set equal to zero, the resulting local liquid phase pressure is given by

$$p_L = \tfrac{1}{10}\epsilon(1-\epsilon)\rho_L (u_G - u_L)^2. \quad [B.7]$$